Tumor Biology and Immunology

Cancer Research

Targeting Brain-Adaptive Cancer Stem Cells Prohibits Brain Metastatic Colonization of Triple-Negative Breast Cancer

Ding Ren[1,2], Xiaoping Zhu[1], Ren Kong[1,3], Zhen Zhao[1,4], Jianting Sheng[1], Jiang Wang[1,5], Xiaoyun Xu[1], Jiyong Liu[1,6], Kemi Cui[1], Xiang H.-F. Zhang[7], Hong Zhao[1], and Stephen T.C. Wong[1,7,8]

Abstract

Triple-negative breast cancer (TNBC) exhibits more traits possessed by cancer stem cells (CSC) than other breast cancer subtypes and is more likely to develop brain metastases. TNBC patients usually have shorter survival time after diagnosis of brain metastasis, suggesting an innate ability of TNBC tumor cells in adapting to the brain. In this study, we establish novel animal models to investigate early tumor adaptation in brain metastases by introducing both patient-derived and cell line–derived CSC-enriched brain metastasis tumorsphere cells into mice. We discovered astrocyte-involved tumor activation of protocadherin 7 (PCDH7)-PLCβ-Ca2+-CaMKII/S100A4 signaling as a mediator of brain metastatic tumor outgrowth. We further identified and evaluated the efficacy of a known drug, the selective PLC inhibitor edelfosine, in suppressing the PCDH7 signaling pathway to prohibit brain metastases in the animal models. The results of this study reveal a novel signaling pathway for brain metastases in TNBC and indicate a promising strategy of metastatic breast cancer prevention and treatment by targeting organ-adaptive cancer stem cells.

Significance: These findings identify a compound to block adaptive signaling between cancer stem cells and brain astrocytes.
Cancer Res; 78(8); 2052–64. ©2018 AACR.

Introduction

Metastatic brain tumors appear in 8%–10% of all cancers. Despite advances in neurosurgery and radiotherapy, few patients live longer than a year. Thus, treatment of brain metastases is considered an unmet medical need. While most brain metastases occur at the advanced stages of cancer progression, triple-negative breast cancer (TNBC) usually spreads to the brain rapidly at earlier stages or even before the diagnosis of primary cancer (1). Increased brain metastases at late tumor development stages are primarily attributed to advances in targeted therapy, which improve the management of systemic disease, but the poor bioavailability of these therapies to the brain increases the brain's potential as a sanctuary site for metastatic disease (2). To this end, targeted therapies with improved brain bioavailability seem promising for disease control (3). However, the treatment for early-developing brain metastases remains a major challenge that limits the patients' outcome.

About 15%–25% of breast cancer are triple negative, that is, estrogen receptor–negative, progesterone receptor–negative, and HER2-negative. TNBCs generally do not respond to targeted treatments, so no strategy exists for prevention and control of TNBC brain metastasis. However, brain metastases have consistently been found with increased frequency in younger and premenopausal TNBC patients (4). The shorter time to development of brain metastases in TNBC and shorter survival time after brain metastasis diagnosis (4) may indicate an innate ability of TNBC tumor cells in adapting to the brain.

Cancer stem cells (CSC), the subpopulation of tumor cells that possess tumor-initiating potential, have been reported to drive tumor metastases (5). The concept of CSCs initiating tumor growth is quite similar to the metastatic process. Although many cells may be shed from the primary tumor, less will survive during circulation to seed a secondary site, and even less will adapt to a new niche and propagate into a clinically apparent tumor (6, 7). CSCs possess enhanced plasticity or adaptive flexibility in their cellular microenvironment (8, 9). Patients with TNBCs whose tumors have more CSC traits than other breast cancers (8, 9) are more likely to develop brain metastases. This led us to hypothesize that brain metastases from TNBC may arise from a brain-tropism CSC population that has enhanced ability to adapt the brain niche.

In our study, patient samples of TNBC brain metastatic tumor and brain-seeking (Br) cell lines were cultured as tumorspheres in

[1]Department of Systems Medicine and Bioengineering, Houston Methodist Research Institute, Weill Cornell Medicine, Houston, Texas. [2]Outpatient Center, PLA NO.85 Hospital, Shanghai, P.R. China. [3]Institute of Bioinformatics and Medical Engineering, School of Electrical and Information Engineering, Jiangsu University of Technology, Changzhou, P.R. China. [4]Department of Radiology, Zhongda Hospital, Medical School of Southeast University, Nanjing, P.R. China. [5]Department of Orthopedics, Tongji Hospital, Wuhan, P.R. China. [6]Department of Pharmacy, Changhai Hospital, Shanghai, P.R. China. [7]Lester and Sue Smith Breast Center, Baylor College of Medicine, Houston, Texas. [8]Houston Methodist Cancer Center, Houston Methodist Hospital, Houston, Texas.

Note: Supplementary data for this article are available at Cancer Research Online (http://cancerres.aacrjournals.org/).

D. Ren, X. Zhu, and R. Kong contributed equally to this article.

Corresponding Authors: Hong Zhao, Houston Methodist Research Institute, 6670 Bertner Avenue, R6-216, Houston, TX 77030. Phone: 713-441-3557; Fax: 713-441-7189; E-mail: hzhao@houstonmethodist.org; and Stephen T.C. Wong, stwong@houstonmethodist.org

doi: 10.1158/0008-5472.CAN-17-2994

neural stem cell conditions to enrich CSC populations. Using sphere-forming assays to assess self-renewal, we showed that brain metastases from TNBC possessed sphere-forming capacity. Intracardiac injection of the patient-derived and Br cell line–derived tumorspheres into immunodeficient mice led to similar multifocal tumor formation and recapitulated tumor cytoarchitecture. Serial injection of patient-derived tumorspheres into mice showed that the putative CSC population can be serially passaged. More importantly, we observed that intracardiac injection of the Br cell line–derived tumorspheres initiated earlier tumor outgrowth in more mice than their corresponding counterpart cell lines, indicating an innate brain-adaptive property of the enriched CSC population.

RNA sequence analysis of the Br cell line–derived tumorspheres versus their corresponding Br counterpart cell lines identified 17 differentially expressed genes. Of these, a brain-specific gene *protocadherin7* (*PCDH7*) that normally has very low expression in human breast tissue, had significantly higher expression in the brain metastatic tumors. High *PCDH7* mRNA expression was significantly correlated with decreased brain metastasis-free survival in a combined breast cancer patient cohort ($n = 368$). PCDH7 is an important contributor to brain metastasis in a syngeneic lung mouse model (10), although the metastases of lung cancer is quite different from that of breast cancer. We further identified that the increased PCDH7 expression in tumor cells, induced by interacting with astrocytes, preserved the stemness and promoted *in vivo* tumor colonization through PCDH7-PLCβ-Ca^{2+}-CaMKII/S100A4 signaling. A known drug for selective PLC inhibition, edelfosine, was administered to mouse models to suppress the signaling activation, and the results showed promising efficacy in preventing brain metastatic colonization. These studies demonstrate promise for targeting brain-adaptive CSCs to prevent or treat TNBC metastases and indicate a possibility of targeting organ-adaptive CSCs to prevent or treat metastasis in general.

Materials and Methods

Cell lines and compounds

MDA-MB-231-Br and CN34-Br human breast cancer Br cell lines were generously provided by Drs. Patricia Steeg (National Cancer Institute. Bethesda, MD) and Joan Massague (Memorial Sloan Kettering Institute, New York, NY). All other cancer cell lines for studying PCDH7 expression were purchased from ATCC. Normal human astrocytes and human brain microvascular endothelial cells were purchased from Lonza Group Ltd. Cell line characterization or authentication was performed with short tandem repeat profiling and passaged in our laboratory for less than 6 months after receipt. All cell lines were tested for mycoplasma negative and maintained at 5% CO_2 at 37°C. Compound ET-18-OCH3 (edelfosine) was purchased from Sigma Aldrich.

Tumorsphere culture and RNA-seq analysis

Two deidentified TNBC patient brain metastatic tissue specimens were collected in accordance with the Houston Methodist Hospital Institutional Review Board. Written informed consent from the patients were obtained and the studies were conducted in accordance with a recognized ethical guideline Declaration of Helsinki. Samples were mechanically dissociated and subjected to enzymatic digestion with 200 μL Liberase Blendzyme (0.2 Wunisch U/mL, Roche) for 15 minutes at 37°C on an incubator rocker (VWR). Undigested tissue was removed, and red blood cells were lysed (RBC Lysis Buffer, Stem Cell Technologies). Cells were washed with PBS, subsequently resuspended in complete NSC (cNSC) media, and plated in an ultra-low attachment plate (Corning). cNSC media is comprised of NSC basal media [1% N2 supplement (Gibco), 0.2% 60 μg/mL N-acetylcystine, 2% neural survival factor-1 (Lonza), 1% HEPES, and 6 mg/mL glucose in 1:1 DMEM and F12 media (Gibco)], supplemented with 1× antibiotic–antimycotic (Wisent), 20 ng/mL human epidermal growth factor (Sigma), 20 ng/mL basic fibroblast growth factor (Invitrogen), and 10 ng/mL leukemia inhibitory factor (Chemicon). We also used two Br cell lines cultured in cNSC media: MDA-MB231-Br and CN34-Br cell lines. Cultures were maintained at 37°C, 5% CO_2, and media were changed every other day, or as needed.

Total RNA of early-passage tumorspheres derived from MDA-MB231-Br and CN34-Br cell lines were isolated with TRI Reagent (Life Technologies) and a RiboPure RNA Isolation Kit (Life Technologies) according to the manufacturer's instructions. rRNA was removed by poly-A selection using oligo-dT beads and mRNA was fragmented and reverse transcribed to yield double-stranded cDNA using random hexamers. cDNA was blunt ended, had an A base added to the 3′ ends, and Illumina sequencing adapters were ligated to the ends. Ligated fragments were amplified for 12 cycles using primers incorporating unique index tags. Fragments were sequenced with an Illumina HiSeq-2000 using single reads extending 50 bases. Raw data were demultiplexed and aligned to the reference genome using TopHat. Transcript abundance was estimated from the alignment files using Cufflinks. EdgeR was used for differential expression analysis.

Sphere formation assay and limiting dilution analysis

Tumorspheres were dissociated using 5–10 μL Liberase Blendzyme in 1 mL of PBS for 5 minutes at 37°C. Cells were plated at limiting dilution (1,000 to 1 cells per well) in 200 μL of cNSC media in quadruplicate in a 96-well plate. After seven days, the number of spheres per well was counted for each dilution, and was used to estimate the mean number of spheres per 2,000 cells. For patient samples, this assay estimated secondary sphere formation, whereas cell lines were of passage three or higher. The fraction of negative wells versus cell dilution was graphed and fitted with a linear regression to estimate stem cell frequency, as in Tropepe and colleagues (11). Following the assumption that a single stem cell gives rise to one sphere, the proportion of negative wells can be defined by the zero point (F_0) of the Poisson distribution: $F_0 = e^{-x}$, where x is the mean number of cells per well. The dilution at which it is expected to have one stem cell (one sphere) per well can be identified by the point at which the line-of-best-fit crosses 0.37 (when $x = 1$, $F_0 = e^{-1} = 0.37$; ref. 11).

Microarray data analysis

Two independent datasets of breast tumor cohorts, "EMC-286" (Erasmus Medical Center, $n = 286$; GSE2034) and "MSK-82" (Memorial Sloan-Kettering Cancer Center; $n = 82$; GSE2603), for which microarray and clinical data (metastasis-free survival time) are publicly available were used for the correlation analysis. Researchers defined metastasis-free survival as the "time from randomization to the first evidence of distant metastatic disease, excluding pelvic lymph nodes, or death from any cause". The classification was implemented in the package "e1071" of R, where the cross-validation for Support Vector Machine (SVM)

was set as five-fold and other parameters for the SVM were set as default. We used the receiver operating characteristic (ROC) method to indicate the performances for the patient classification. The area under the ROC curve (AUC) illustrates the accuracy of the classification. Furthermore, we did the brain metastasis-free survival time analysis based on the PCDH7 expression for the breast cancer patients. The survival analyses were implemented in the "survival" package of R. GSE26291 dataset was used to analyze the gene expression of calcium ion channel-related genes, epithelial–mesenchymal transition–related genes, cell survival and apoptosis genes, in the MDA-MB-231 tumor cells after coculturing with murine astrocytes for 72 hours, comparing with the tumor cells coculturing with NIH 3T3 cells.

Oncomine platform data analysis

Relative levels of *PCDH7* mRNA expression in normal human tissues were obtained by Oncomine Cancer Microarray database analysis (http://www.oncomine.com). The data were $\log_2$ transformed, with the media set to zero and SD set to one. Molecular concept analysis of the differentially expressed 17 genes in tumorspheres was performed using Oncomine platform software.

General animal study procedures

Animal procedures were conducted under the approval of Institutional Animal Care and Use Committee of Houston Methodist Research Institute. For *in vivo* imaging, all tumor cell lines were stably transduced with Firefly luciferase (F-luc) and EGFP. Female NOD-SCID mice (6–8 weeks-of-age; Charles River Laboratories) were anesthetized with isoflurane/O_2 and injected in the left cardiac ventricle with tumor cells (1.75×10^5 cells in 0.1-mL PBS). Tumor cell growth was monitored by repeated noninvasive bioluminescence imaging twice per week using an IVIS 200 system (Xenogen). "Brain metastasis-free survival" was defined as the interval from tumor cell injection until the emergence of brain metastatic bioluminescent signals in mouse brain. *In vivo* compound treatment with the PLC-selective inhibitor ET-18-OCH3 (i.p., once daily, 30 mg/kg/day) started 10 days after tumor cell injection. Mouse physical conditions were monitored once daily and animals were euthanized with CO_2 asphyxiation when neurologic impairment was evident or physical condition scores were ≤ 2. Whole brains were removed and 10-μm brain sections were serially cut. One section for every 100 μm was stained with hematoxylin and eosin or anti-CD34, anti-Ki67, anti-pPLCβ, and anti-PCDH7 according to standard procedures. Whole-slide montage images were acquired with an Olympus IX81 automatic microscope (HMRI Advanced Cellular and Tissue Microscope Core Facility) and a software algorithm that we developed was used for segmentation and quantification analysis (12).

Intravital two-photon microscope imaging

Considering a closed window will better preserve the physiologic microenvironment for tumor cells and cause less damage to mouse for the long-time imaging, we chose to establish the closed thinned-skull window. Surgery was done under aseptic conditions. The mouse's head was fixed by a stereotactic apparatus. The skin on top of the frontal and parietal regions of the skull was cleaned with antimicrobial betadine solution. A longitudinal incision of the skin was made between the occiput and forehead. The skin was then cut in a circular manner on top of the skull, and the periosteum underneath was scraped off to the temporal crests. A 5×5 mm square was drawn over the frontal and parietal regions of the skull. Using a high-speed air-turbine drill (CH4201S; Champion Dental Products) with a burr tip size of 0.5 mm in diameter, a groove was made on the margin of the drawn square. This groove was made thinner by cautious and continuous drilling of the groove but not drilling through the skull. Then, the same cautious drilling procedure was applied to thin the skull within the groove area until the skull becomes transparent and the vessels are visible. Cold saline was applied during the drilling process to avoid thermal injury of the cortical regions. A cover-glass was then glued on top of the skull for three purposes, (i) provide rigidity, (ii) inhibit bone regrowth, and (iii) reduce light scattering from irregularities on the bone surface. Imaging depths of up to 250 μm below the cortical surface can be achieved using two-photon laser scanning microscope. The surgery took an hour in each case, the animal was positioned on a heating pad (37°C) during the surgery and until they recovered from the anesthesia. A total of 1×10^5 tumor cells in 20-μL PBS were injected through a biocompatible microrenathane catheter (Braintree Scientific Inc.) into the common carotid artery, and a 3-mm length catheter "stent" was secured in place with two sutures to reestablish blood flow to the carotid artery.

Intravital two-photon imaging of tumor-bearing mice was performed with an Olympus FV1000-MPE microscope with a 25×, 1.05 NA water immersion objective with a correction collar. The laser-light source consisted of a standard femtosecond-pulsed laser system (Mai Tai HP with DeepSee, Newport/Spectra-Physics) for excitation of fluorophores (740–950 nm). Fluorescent signals were collected via a dichroic mirror (DM670LP) and sent to photomultiplier tube (PMT) detectors behind appropriate filter cubes to quantify GFP and Texas Red. Texas Red dextran (70 kDa, Invitrogen, catalog # D1830) was used to identify the vasculature. We initially imaged 10–15 random fields (512×512 μm at 512×512 pixels) for a depth of 50–250 μm using 5-μm steps beginning at the brain surface, followed by 4–6 cortical regions of interest, where tumor cells were visible, over time (days 1, 3, 6, 10, and 14). If tumor cells disappeared in one area, we imaged this area a final time, and then selected another area of interest and followed. We retrieved the same cells over time using vascular patterns and unique branch points of the cortical vasculature as landmarks.

Image analysis

Images were reconstructed in 3D and through time using Image J. We quantified 108 individual metastasizing cells in the PCDH7shRNA cell line ($N = 6$ mice) and 102 in the control cell line ($N = 5$ mice) over 14 days. In addition, we imaged cancer cells for 30–60 minutes directly after intra-arterial injection (PCDH7shRNA: 58 cells, $N = 4$ mice; control: 69 cells, $N = 4$ mice). We measured the same brain regions over time and quantified for each metastatic nodule: from day 1, for each individual cancer cell over time, we noted that a fraction of cancer cells were intravascular, extravasated, and perivascular as single cells, and perivascular as multiple cells (≥ 4). Dormant cells were noted during the experiment. Only cancer cells directly contacting a vessel were "perivascular." Dormancy was defined as lack or arrest of cancer cell proliferation without signs of regression during the duration of one experiment. Micrometastases were defined as multicellular cancer cell clusters of 4–10 cells (generally indicates a metastasis diameter of <50 μm), and macrometastases

as clusters of >10 cells (>50 μm). These are mouse tumor equivalents of an MRI-detectable human brain metastasis (5 mm).

Statistical analysis

Data are expressed as means ± SEM. To compare groups, we used the Student's two-tailed *t* test or the ANOVA with *post hoc* test (Figs. 3C, 4G, and 5E). To assess correlations, we calculated the Spearman rank correlation coefficient. To compare frequencies of metastasis and metastasis-free survival, we used Fisher exact test and log-rank test. $P < 0.05$ was regarded as statistically significant. We performed all calculations with SigmaPlot statistical software (version 11.2; Systat Software Inc.).

Results

Patient brain metastatic tumor and Br cell lines form self-renewable tumorspheres

We obtained fresh brain metastases tissue from two TNBC patients and cultured them as primary and then secondary tumorspheres in neural stem cell media. As a sphere is considered to represent all progeny from a single stem cell, tumorsphere formation reflects the presence of a stem cell population (11). We observed that the second sphere-forming efficiencies of the patient tissue were 27 spheres/2,000 cells (SD = 21) and 11 spheres/2000 cells (SD = 3.4; $P = 0.39$), where secondary sphere formation is a hallmark of the self-renewal property of stem cell (13). Stem cell frequency was estimated via limiting-dilution analysis, and the median frequencies for the two patient samples were 1 sphere/127 cells (range 1/35–1/217 cells) and 1 sphere/200 cells (range 1/125–1/256 cells); they were not statistically different ($P = 0.40$). We supplemented our work with representative human breast cancer Br cell lines. The MDA-MB-231-Br and CN34-Br are both derived from brain metastases originating from TNBC tumors (14). Both cell lines formed spheres [MDA-MB-231-Br, 153 spheres/2,000 cells (SD = 94); CN34-Br, 53 spheres/2,000 cells (SD = 13)], and their sphere-forming capacity is higher than that of cultured patient samples, which may due to prolonged culture in increasing stem cell frequency (15), as evidenced by frequencies of one sphere/18 cells and one sphere/40 cells for MDA-MB-231-Br and CN34-Br cultures, respectively. Despite the increase in sphere-forming capacity, the Br cells lines and patient brain metastases–derived tumorspheres were of similar morphology and size (Fig. 1A).

Breast tumors from patients with the brain as the first metastatic site were negative for estrogen and progesterone receptor but frequently expressed CK5, nestin, and prominin-1 (CD133; ref. 16). Interestingly, both nestin and CD133 are considered to be CSC markers for glioblastoma (17). Similarly, an *in vitro* selection of a CSC population from the TNBC cell line identified CD133 and CD44 as marker proteins for these cells (18). We examined the expressions of these markers in the patient-derived spheres (CK5, nestin, CD133, and CD44; Fig. 1B), correlating with the presence of a stem-like population.

Patient-derived tumorspheres are serially transplantable in mice and form intraparenchymal multifocal tumors

The gold standard for identification of a CSC population is serial tumor formation in immunocompromised mice (19). As the brain lacks a lymphatic system, cancer cells can only metastasize to the brain via the blood stream (20). We thus performed serial intracardiac injections into NOD-SCID mice using patient-derived tumorspheres to assess their ability to be serially passaged *in vivo*. Two parental (P0) tumors were cultured into tumorspheres to select for CSCs. Three mice each were injected with 1.75×10^5 P0 tumor cells ($n = 6$ total). Each P0 derivative from the subsequent (S1) tumors was similarly cultured and injected to give rise to S2 tumors ($n = 6$ total). The two patient P0 tumors derived S1 and S2 tumors in all 12 mice, forming intraparenchymal multifocal masses, and the tumor cells are cohesive, cuboidal, or columnar cells arranged in sheets, tubules, or acinar structures, and have moderate-to-abundant cytoplasm (Fig. 1C and D). The tumor growth was primarily observed around small blood vessels (co-option; Fig. 1E). This is consistent with clinical presentation of brain metastases from breast cancer, which are typically multifocal and intracerebral, and less commonly solitary and leptomeningeal. Both S1 and S2 tumors ($n = 4$) were stained with the same markers used to clinically diagnose patient brain metastases, that is, cytokeratin 7 (CK7), ER, PR, and HER2. The CK7-positive and ER/PR/HER2–negative staining profiles and patterns in the S1/S2 tumors were identical to those of the original patient brain metastasis (Fig. 1F). The expressions of nestin and CD44 were abundant in the S1/S2 tumors, and CD133 and CK5 were moderately expressed (Fig. 1F). These indicate that injection of brain metastasis tumorspheres in mice recapitulate the patient tumors; it also demonstrates that tumorspheres possess the CSC capacity to differentiate into various tumor cell types *in vivo*.

Br cell line–derived spheres exhibit enhanced capacity in inducing brain metastases than their counterpart cell lines

The Br cell lines and the derived tumorspheres have stable luciferase expression, which enables us to concurrently compare their brain metastatic kinetics *in vivo*. Although brain metastasis occurred in all the mice injected with Br cells or tumorsphere cells (MDA-MB-231-Br and CN34-Br) at the same cell number of 1.75×10^5 or 1.75×10^4, the tumorsphere cells initiated brain metastases earlier ($P < 0.001$; Fig. 1G–I). However, our data could not show that the tumorsphere cells are more tumorigenic at lower numbers than their Br counterparts, because injection of low number cells (1.75×10^3 and 1.75×10^2) failed to induce brain metastasis in almost all mice with tumorsphere or Br cell injection. It is likely due to the limited tumor cell arrest at blood vessels and the low efficiency of metastatic outgrowth. It has been reported that 8%–10% of the total injected tumor cells are able to arrest at the blood vessel branches when injected through carotid artery (7), and the rate is expected to be even lower when injected through left ventricle. Furthermore, >95% of the arrested cells will die during development and only less than 5% cells will continue to grow into macrometastasis (7, 21). Nonetheless, the data showing earlier detection of brain metastases in 100% of mice with the tumorsphere cells compared with regular Br cells suggest that the CSCs have an enhanced adaptation ability to colonize in the brain.

High PCDH7 expression in brain metastases

We performed RNA sequence analysis of the early-passage tumorspheres derived from both MDA-MB-231-Br and CN34-Br cell lines. Comparison of the common differentially expressed genes between the two lines identified 16 upregulated genes in both tumorspheres relative to the Br cells ($P < 0.01$,

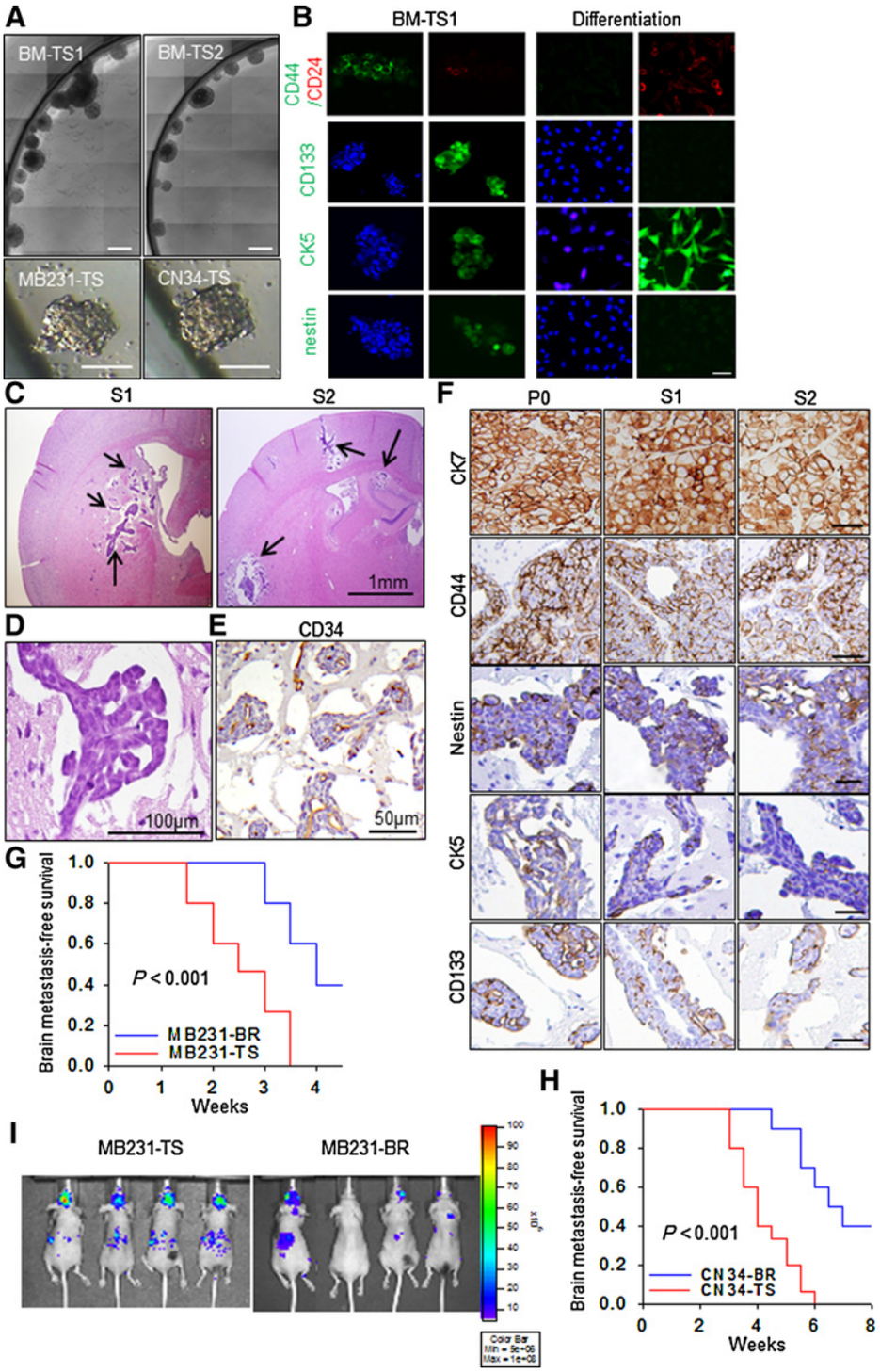

Figure 1.
Brain metastasis models derived from brain metastasis–derived tumorspheres. **A,** Bright-field images of representative tumorspheres cultured from fresh brain metastases tissue from two TNBC patient undergoing neurosurgical resection, that is, BM-TS1 and BM-TS2, and Br cell lines, that is, MDA-MB-231-TS and CN34-TS. Scale bar, 50 μm. **B,** The BM-TS1 tumorspheres were stained with antibodies to CD44, CD24, CD133, CK5, and nestin. For differentiation, BM-TSs were disrupted and the cells plated onto glass coverslips in medium supplemented with 5% FCS. After 10 days of adherent culture, the cells were stained with the same antibodies. Scale bar, 20 μm. **C,** Representative hematoxylin and eosin staining images showing the intraparenchymal multifocal S1 and S2 brain metastatic tumors in mice. Mice were injected with 1.75×10^5 BM-TS–dissociated cells through the left ventricle. **D,** The cytoarchitecture of the S1/S2 tumor. **E,** The vessel cooption growth pattern of the S1/S2 tumors. **F,** The expression pattern of CK7, CD44, nestin, CK5, and CD133 in the original patient P0 brain metastatic tumor and serially passaged S1 and S2 tumors. **G** and **H,** Kaplan–Meier survival curves for brain metastasis-free survival of tumorsphere-derived models (MB231-TS, CN34-TS) in comparing with Br cell line–derived models (MB231-Br, CN34-Br). *P* values were determined by log-rank test. $N = 10$ in each group. **I,** The representative bioluminescent imaging of the brain metastases in MB-231-TS and MB-231-Br models.

Supplementary Table S1), and 1 downregulated gene in both tumorspheres, that is, *STC1*. Interestingly, the molecular concept analysis using Oncomine platform software showed that the 16 genes have a strong association with the literature-based concept of molecular signature of human embryonic stem cells ($P = 7.69E{-}6$, $Q = 0.01$; ref. 22).

Among the 17 genes, PCDH7 is the only one that normally expresses exclusively in human central nervous system (Fig. 2A; Supplementary Fig. S1A) and mouse brain (23). Upregulated mRNA expression of PCDH7 was reported in both MDA-MB-231-Br and CN34-Br cell lines (14). PCDH7 protein was highly expressed in the derived tumorspheres: 5.5-fold higher than

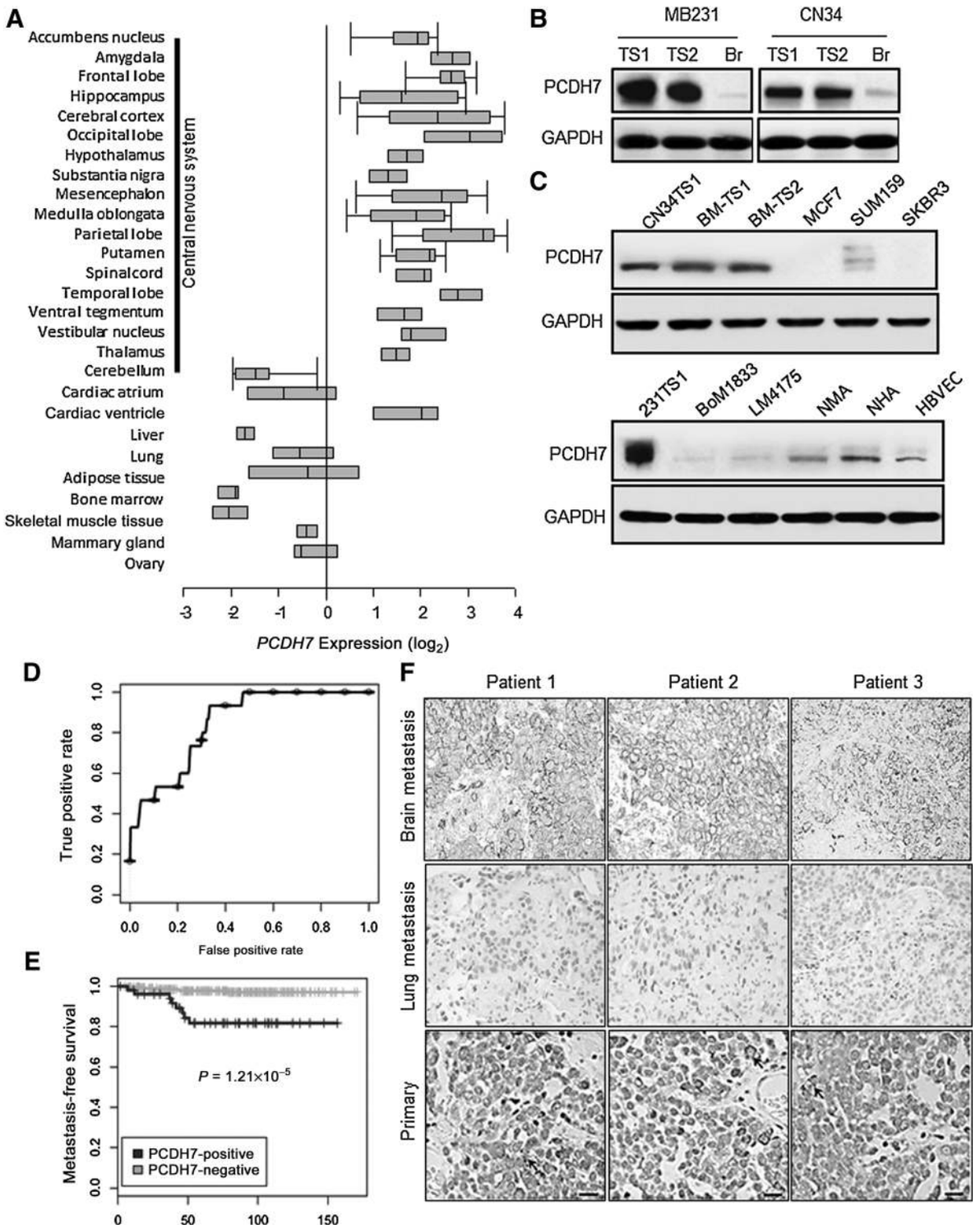

Figure 2.

High expression of PCDH7 in brain metastasis. **A,** Oncomine database analysis of *PCDH7* expression in normal human tissue (50). **B,** Western blot analysis of PCDH7 in independent brain metastasis-derived tumorspheres (TS1 and TS2) and corresponding Br cell lines. **C,** Protein expression of PCDH7 in TNBC patient brain metastasis tumorspheres (BM-TS1 and 2) and various cell models. MCF7, SUM159, SKBR3: human breast cancer cell lines; BoM1833, MB231 bone-seeking cell line; LM4175, MB231 lung seeking cell line; NMA, primary normal mouse astrocytes; NHA, normal human astrocytes; HBVEC, human brain microvascular endothelial cells. **D,** ROC curve for PCDH7 expression in primary breast tumor samples of brain metastatic patients using the combined 368 microarray data (MSK-82 and EMC-286 cohort). **E,** Kaplan–Meier curves showing the brain metastasis-free survival of patients with positive or negative PCDH7 expression in the combined cohort of 368 breast cancer patients. $P = 1.21 \times 10^{-5}$ determined by log-rank test. **F,** Representative PCDH7 IHC staining of matched patient tissue sections of brain metastasis, lung metastasis, and primary breast tumors. Scale bar, 20 μm.

MDA-MB-231-Br ($P = 0.004$) and 4-fold higher than CN34-Br ($P = 0.008$; Fig. 2B). PCDH7 is also highly expressed in TNBC patient brain metastasis-derived tumorspheres and moderately expressed in normal human and mouse astrocytes (NHA and NMA), and human brain microvascular endothelial cells (HBVEC; Fig. 2C). However, other members in the PCDH family are not differentially expressed between tumorsphere and Br cells (Supplementary Fig. S1B).

To explore the clinical relevance of *PCDH7*, we retrospectively studied breast cancer patients and noted high *PCDH7* mRNA expression significantly correlated with brain relapses (AUC = 0.849, Fig. 2D) and decreased brain metastasis-free survival ($P = 1.21 \times 10^{-5}$, Fig. 2E) in a combined breast cancer patient cohort ($n = 368$, EMC-286+MSK-82). *PCDH7* expression was not correlated with bone or lung metastasis in these clinical cohorts (Supplementary Fig. S1C and S1D). We further measured PCDH7 protein in 34 primary breast tumors and 29 brain metastatic tumors of TNBC patients (4 are matched samples with both primary and brain tumors; Fig. 2F). Most of the brain metastatic samples (27/29) had strong PCDH7 staining (H score 3+, see Materials and Methods), including 4 samples with matched primary tumors, and the 2 remaining samples had intermediate immunoreactivity (H score 2+). Three of the 4 matched primary tumors had sporadic staining for PCDH7, whereas 91% (31/34) of primary breast cancer samples were negative for PCDH7 (H score 0 and 1+; Supplementary Table S2). In addition, PCDH7-positive staining was not observed in the nine lung metastatic tissue samples (Fig. 2F). Thus, PCDH7 may be a key contributor to TNBC brain metastases.

Functional role of PCDH7 in brain metastasis

To determine the functional involvement of PCDH7 in brain metastasis, knockdown of PCDH7 by shRNAs and rescue of PCDH7 gene expression in brain metastatic tumorspheres were performed (Supplementary Fig. S2A and S2B). Tumorsphere cells (1.75×10^5) with knockdown PCDH7 (PCDH7 shRNA), rescued PCDH7, or control shRNA were injected into the left ventricle of mice. In the MDA-MB-231-Br tumorsphere model, three weeks after cell inoculation, 70% of mice injected with control shRNA cells had detectable brain metastases, but no PCDH7 shRNA mice did ($P < 0.001$; Fig. 3A, left). Then, five weeks after inoculation, all controls had brain metastases, but only 4 in the PCDH7 shRNA group developed brain metastases by 6 weeks postinoculation. Forty percent of the mice in the PCDH7 shRNA group had no brain metastasis as confirmed by histology until the end of 8 weeks. Furthermore, knockdown of PCDH7 decreased metastatic lesion numbers and areas in mouse brain sections ($P < 0.05$, Fig. 3B; Supplementary Table S3). Delay and prevention of brain metastases by PCDH7 knockdown occurred similarly in the CN34-Br tumorsphere mouse model (Fig. 3A-right). Mice injected with PCDH7-rescued cells had brain metastases similar to controls (Fig. 3A and B). Knocking down PCDH7 did not modify mammary tumor growth and lung colonization *in vivo* (Supplementary Fig. S2C and S2D). These findings further confirm that PCDH7 is a key player in brain metastatic formation.

We then evaluated the role of PCDH7 in specific brain metastatic steps. We found that knockdown of PCDH7 decreased tumor cell extravasation through an *in vitro* blood–brain barrier system and in mouse brain (Fig. 3C–E). Furthermore, as examined by intravital two-photon microscope, the PCDH7 shRNA cells showed a significant defect in tumor colonization (Fig. 4A–D), which is the rate-limiting step in metastases (24). Two weeks after injection, most of the arrested PCDH7 shRNA tumor cells either disappeared (74%) or remained as solitary cells (18%), whereas 70% of the extravasated control shRNA tumor cells developed into multicellular loci ($\geq$4 cells). Neither PCDH7 knockdown nor transduction significantly changed *in vitro* tumor cell proliferation (Supplementary Fig. S2E and S2F), prompting us to study brain microenvironment elements that may stimulate PCDH7-mediated tumor colonization.

PCDH7-mediated tumor–astrocyte interaction retains CSC self-renewal and activates PLCβ-Ca^{2+}/CaMKII/S100A4 signaling

Immuno-reactive PCDH7 expression was detected in brain metastases in the PCDH7 shRNA group, as well as the tumor surrounding astrocytes (Fig. 3B). The reexpression of PCDH7 in the survived brain metastatic tumor cells may implicate that the tumor cells are required to adapt to express PCDH7 to survive in the brain. We found that when the primary MDA-MB-231 cells were cocultured with astrocytes, the expression of *PCDH7* in MDA-MB-231 cells was markedly upregulated (Supplementary Fig. S3A; GSE26291). Both mouse and human astrocytes moderately express PCDH7 (Supplementary Fig. S2C), and astrocyte activation was observed in brain metastases (Supplementary Fig. S3B; ref. 25). Human astrocytes facilitated retention of self-renewal for tumorspheres as evidenced by an assay of serial nonadherent passages. Tumorspheres could be propagated beyond passage 5 when cocultured with astrocytes, but sphere cell viability was diminished by passage 2 when cocultured with normal fibroblasts; further propagation was not possible in suspension culture (Fig. 4E). Tumorspheres and astrocytes, when grown on suspension culture, formed heterotypical spheres (Fig. 4F) that required enzymatic and mechanical disaggregation to obtain a single-cell suspension before subculturing. This likely reflects the presence of proper cell–cell interactions among them. Application of neutralizing anti-PCDH7 antibody into the culture media not only disrupted the tumor–astrocyte heterotypical spheres, but also reduced the propagation of the spheres (Fig. 4G).

Protocadherins mediate cell–cell adhesion (26), and a recent study shows that breast and lung cancer cells express PCDH7, mediating the assembly of tumor–astrocyte gap junctions to activate astrocytes in supporting tumor growth (10). In addition, studies indicate that protocadherins are functionally important in relaying signals to cytoplasm (26). To explore whether the PCDH7 cytoplasmic signals are important to brain metastases, we transduced either a full-length *PCDH7* gene (FL-PCDH7) or only the extracellular domain (EC1-3) of the *PCDH7* gene (EC-PCDH7) into tumor cells (Supplementary Fig. S3C), to assess tumor cell colonization and interactions with astrocytes. In animal studies, exclusive and strong astrocyte activation was seen in close proximity of cancer cells even on day 3 post cancer cell injection. We did not observe significant differences in astrocyte response in the EC-PCDH7-injected animals compared with FL-PCDH7–injected animals (Supplementary Fig. S3D). However, four weeks after cell injection, 90% of the arrested or extravasated FL-PCDH7 tumor cells developed into multicellular loci ($\geq$4 cells), while only 22% of the injected EC-PCDH7 tumor cells did (Fig. 5A and B), suggesting that the cytoplasmic signals of PCDH7 are essential for tumor colonization.

PCDH7 proteins mainly localize to cell membrane with some in the cytoplasm and nucleus of a brain metastatic tumorsphere cell (Supplementary Fig. S3E). Similar to other protocadherins,

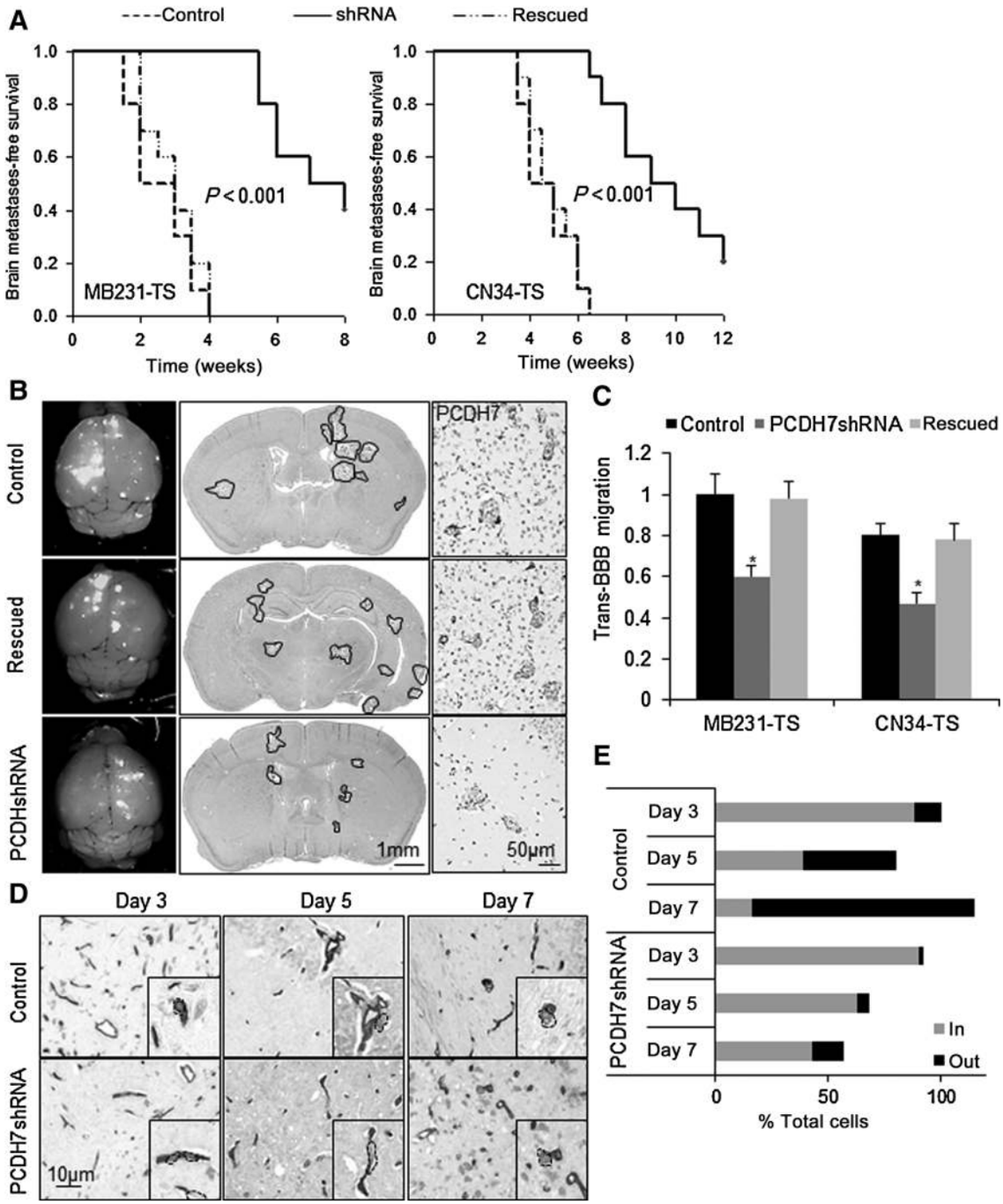

Figure 3.

Functional roles of PCDH7 in brain metastasis. **A,** Kaplan–Meier curves for brain metastasis-free survival of mice injected with tumorsphere cells derived from MB231-Br (left) or CN34 = Br (right) models expressing the shRNA targeting PCDH7, the control shRNA, or the PCDH7 rescued. $n = 10$ mice per group. P value was determined using log-rank test. **B,** Representative images showing metastatic lesions in mouse whole brain (left), hematoxylin and eosin–stained brain section (middle), and PCDH7 immunoreactivities in the brain metastases (right). It was noted that high expression of PCDH7 in both tumor cells and surrounding astrocytes in control group was diminished by PCDH7 shRNA. $n = 5$ mice per group. **C,** Transmigration of the indicated cells through the *in vitro* blood–brain barrier system. *, $P < 0.05$ versus control shRNA. **D,** Representative images showing intravascular and extravasated tumor cells in mouse brain sections. MB-231-TS cells were visualized on 10-μm–thick brain sections by anti-human CD44 and blood vessels by anti-mouse CD34 using IHC. Black rectangles are higher magnification single cell images. $CD44^+$ tumor cells were segmented by dash lines. **E,** Percentage of cancer cells located inside (in) versus outside (out) blood vessels at indicated days after intracardiac tumor cell injection. Intravascular and extravasated tumor cells were counted in every fourth section throughout the entire mouse brain. Data was relative to "control group day 3." It was noted that the % total cells > 100% is due to the cell proliferation, and the % total cells < 100% is due to cell disappearance. $n = 3$ mice per each time point.

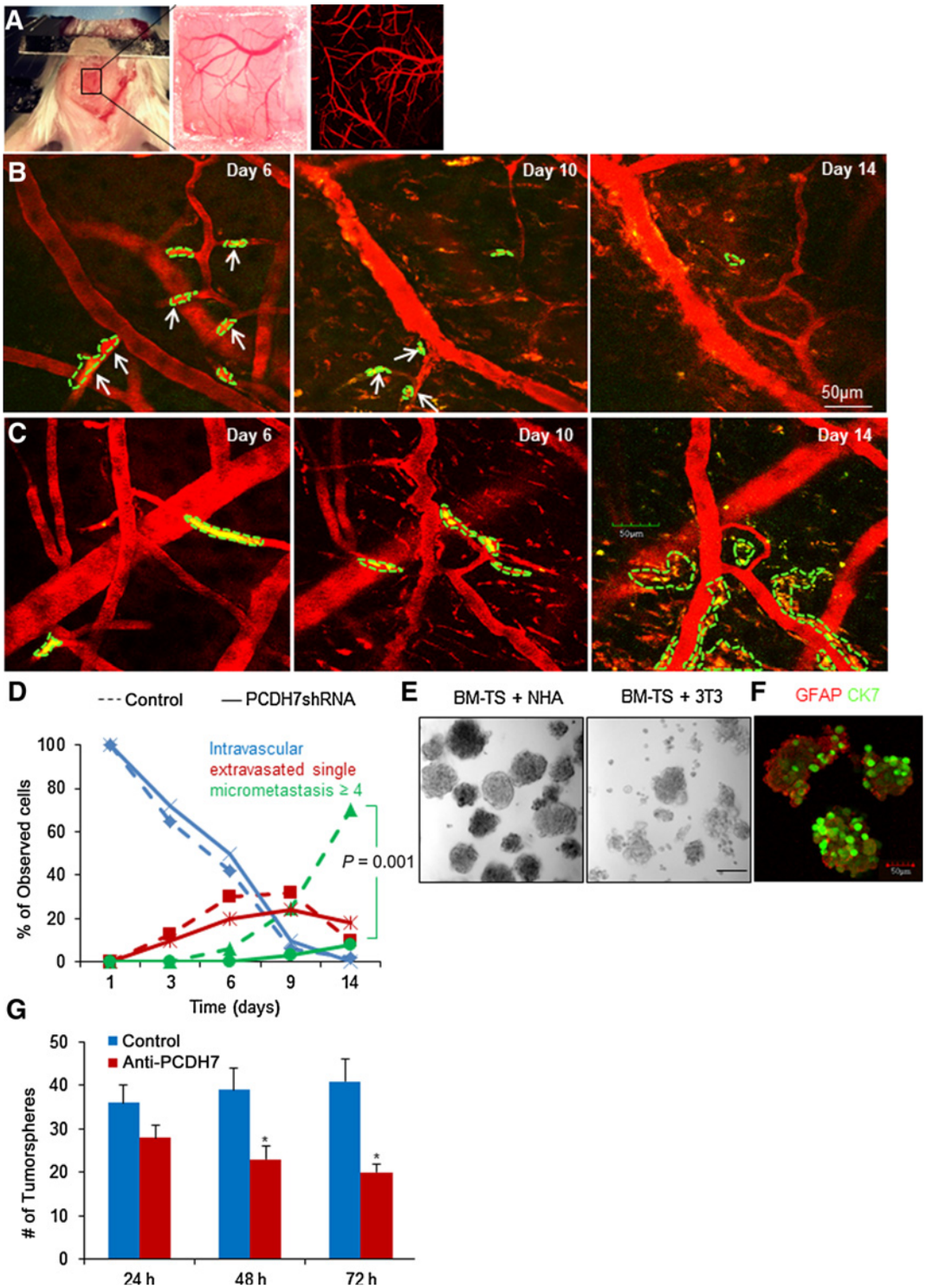

Figure 4.

PCDH7 mediates the interaction between cancer cells and astrocytes to promote tumor colonization. **A,** A thinned-skull window with perfused brain vessels (Texas Red dextran, red). **B** and **C,** Intravital two-photon microscopy images showing tumor cell arrest and extravasation in mouse brain at day 6 and disappearance at day 10 and day 14 (solid white arrows) for PCDH7shRNA MB231-TS cells (**B**), while the control shRNA cells formed colonization at day 14 (**C**). It was noted that the blood vessels became tortuous and leaky after day 6 and remodeled at day 14. **D,** Extravasation and colonization of the indicated cells in mouse brain over time. $n = 4$ mice per group. **E,** Representative bright-filed images of tumorspheres at passage 2 when coculturing BM-TS cells with NHA or normal fibroblasts 3T3 cells. **F,** Representative immunofluorescent images showing the heteotypic spheres formed by cancer cells (stained for CK7) and astrocytes (stained for GFAP). **G,** Effects of PCDH7 neutralization by anti-PCDH7 antibody (1:100) on tumorsphere formation (diameter >50 μm) in the dissociated BM-TS cells and NHAs coculturing system. *, $P < 0.05$ versus control.

PCDH7 has a small serine-rich domain in its COOH terminus that is homologous to the β-catenin binding site of classical cadherins (Supplementary Fig. S3F). Although PCDH7 binds β-catenin directly (Supplementary Fig. S3G), nuclear β-catenin translocation and significant increases of wnt-signaling transcriptional factors (Tcf-4 and Lef-1) were not observed in the tumorsphere cells when cocultured with astrocytes (Supplementary Fig. S3H–S3J), suggesting that the canonical Wnt signaling was not functional in enhancing brain metastatic tumor cell colonization.

Instead, an increased cytoplasmic Ca^{2+} (~30%) was observed independent of PCDH7 expression in the tumorsphere cells (Fig. 5C). Extensive data suggest that tumor cell proliferation is stimulated by a persistent Ca^{2+} increase in contrast to the transitory increase of Ca^{2+} that induces activation of the mitochondrial apoptotic pathway (27). PCDH7 has been shown to mediate the assembly of carcinoma–astrocyte gap junctions (10), and thus allows transmitting Ca^{2+} between astrocytes and brain metastatic tumor cells (25). In response to Ca^{2+} influx from astrocytes (25), we noted a consistently high expression and activation of phosphodiesterase beta (PLCβ) in tumorsphere cells and high expression of downstream calmodulin-dependent protein kinase II (CaMKII) and S100A4 (Fig. 5D). PLCβ catalyzes hydrolysis of phosphatidylinositol 4,5-bisphosphate (PIP2) to inositol 1,4,5-trisphosphate (IP3) and 1,2-diacylglycerol (DAG). Signaling pathway activation of PLCβ-IP3 or PLCβ-DAG is important for transient calcium influx-induced intracellular Ca^{2+} storage, which leads to activation of Ca^{2+}/CaM-dependent kinase and nuclear transcription factors, stimulating maintenance of pluripotency and proliferation of stem cells (28). PLCβ1, CaMKII, and S100A4 activations were also noted in FL-PCDH7 but not EC-PCDH7–transduced tumor cells when coculturing with astrocytes (Fig. 5D).

We pharmacologically suppressed the PCDH7-PLCβ-Ca^{2+}/CaMKII/S100A4 signaling by administering ET-18-OCH3 (edelfosine), a specific PLC inhibitor drug, to the MDA-MB-231-Br tumorsphere xenograft mice. To recapitulate human disease where brain metastatic tumors are established before treatment, we treated mice beginning at day 11 when micrometastatic lesions were detected in the mouse brain at day 10 (Fig. 3A). During the 15-day treatment, brain metastatic tumor growth was significantly inhibited in the ET-18-OCH3 group ($P = 0.04$, Fig. 5E), and the formation of macrometastases (>50 cells) in the treated mice was inhibited by 96% at the end of the 15-day treatment ($P < 0.01$, Fig. 5F and G), that is, the vehicle-treated mice developed 22.5 ± 3.5 whole-brain macrometastases while it was only 1 ± 0.7 in the ET-18-OCH3–treated mice. Meanwhile, activations of cellular PLCβ and tumor cell proliferation were repressed remarkably (Fig. 5H and I). Because of the limited availability of the patient-derived tumorspheres, only *in vitro* tumorsphere treatment was performed and ET-18-OCH3 showed a dose-dependent inhibition on secondary tumorsphere formation (Supplementary Fig. S4A–S4D). These results indicate the potential of targeting PCDH7-PLCβ-Ca^{2+}/CaMKII/S100A4 signaling in inhibiting brain metastases.

Discussion

In this study, we identified a novel signaling pathway for brain metastatic outgrowth of TNBC and presented a new strategy for preventing or combating breast cancer metastasis via targeting organ-adaptive CSCs. We extracted a CSC population from brain metastases and demonstrated that this CSC population has an enhanced brain-adaptive capacity and engages in brain metastatic colonization, the rate-limiting event in brain metastasis (24). Further exploration of the CSC adaptation and colonization signals identified the astrocyte-involved PCDH7-PLCβ-Ca^{2+}-CaMKII/S100A4 pathway. Suppressing the pathway's activation by an old drug, edelfosine, showed obvious efficacy in prohibiting brain metastasis in mouse models.

Several studies suggest that CSCs of primary breast tumors are intrinsically invasive and metastatic *in vivo* (29, 30), while others propose that migratory cells can acquire self-renewal and tumorigenic capabilities through an epithelial–mesenchymal transition (31, 32). In either case, the CSC population is characterized by adaptability to various microenvironments (33). To this end, we hypothesized that if any CSCs exist in brain metastasis, they would evolve to be more adaptive to the brain than their non-CSC counterparts. Thus, we used a "brain-friendly" culture condition (neurosphere media) to enrich the CSC population in brain metastases and demonstrated that brain metastases possess such CSC populations, that is, they have sphere-forming capacity and are able to initiate tumor growth, reproduce original tumor heterogeneity through *in vivo* differentiation, and can be serially passaged *in vivo*. Culturing the Br cell lines in the same media also led to an enriched CSC population, and even more importantly, we were able to directly compare the functions of the paired CSCs with non-CSCs. We found that the CSC population was engaged in the brain metastatic tumor growth with much less latency and faster proliferation than the non-CSC counterparts, suggesting their intrinsic capacity in initiating brain metastasis. Through application of the CSC model, our study provides a much-needed method to study tumor adaption and explore novel metastasis mechanisms. To date, tumorspheres have been successfully cultured from various organs of cancer or metastases (34), including bone marrow, lung tissue, and pancreatic, prostate, melanoma, and ovarian cancers, suggesting an applicable generalization of using tumorsphere CSC models to study organ-specific tumor adaptation signals in metastasis.

Metastatic environment may lead to the development of organ-adaptive tumor cells, which is crucial for tumor cell thriving and surviving (35). In our study, the brain niche endows an enhanced PCDH7 expression on the survived brain metastatic CSCs, which promoted the formation of tumorspheres and retained their self-renewal. Brain cells corresponding to stromal cells are astrocytes, which are the most abundant cell type in the human brain and perform a variety of functions. It is reported that small noncoding RNAs, in particular miRNAs, act nonautonomously spreading from astrocytes to tumor cells by exosomes (36) or cell-to-cell contact (25, 37) to enhance tumor proliferation and reduce apoptosis. Several miRNAs have recently been identified as potential regulators of *PCDH7* in cancer, for example, miR-19a, miR-32, miR-124a, miR-130b, miR-148a, and miR-583 (38). MiR-19a and miR-32 were also defined as glia-enriched miRNAs in brain regulating glia cell type–specific phenotypes (39). The roles of miR-19a and miR-32 in direct or indirect upregulation of *PCDH7* in brain metastatic tumors warrant further studies. In addition, intercellular transfer of calcium, a ubiquitous second messenger, from astrocytes to tumor cells were previously examined (25), and calcium transients can increase the efficiency of gene expression and drive transcription of specific genes (40). These include *PCDH* family genes and genes regulating stem cell differentiation and proliferation (28).

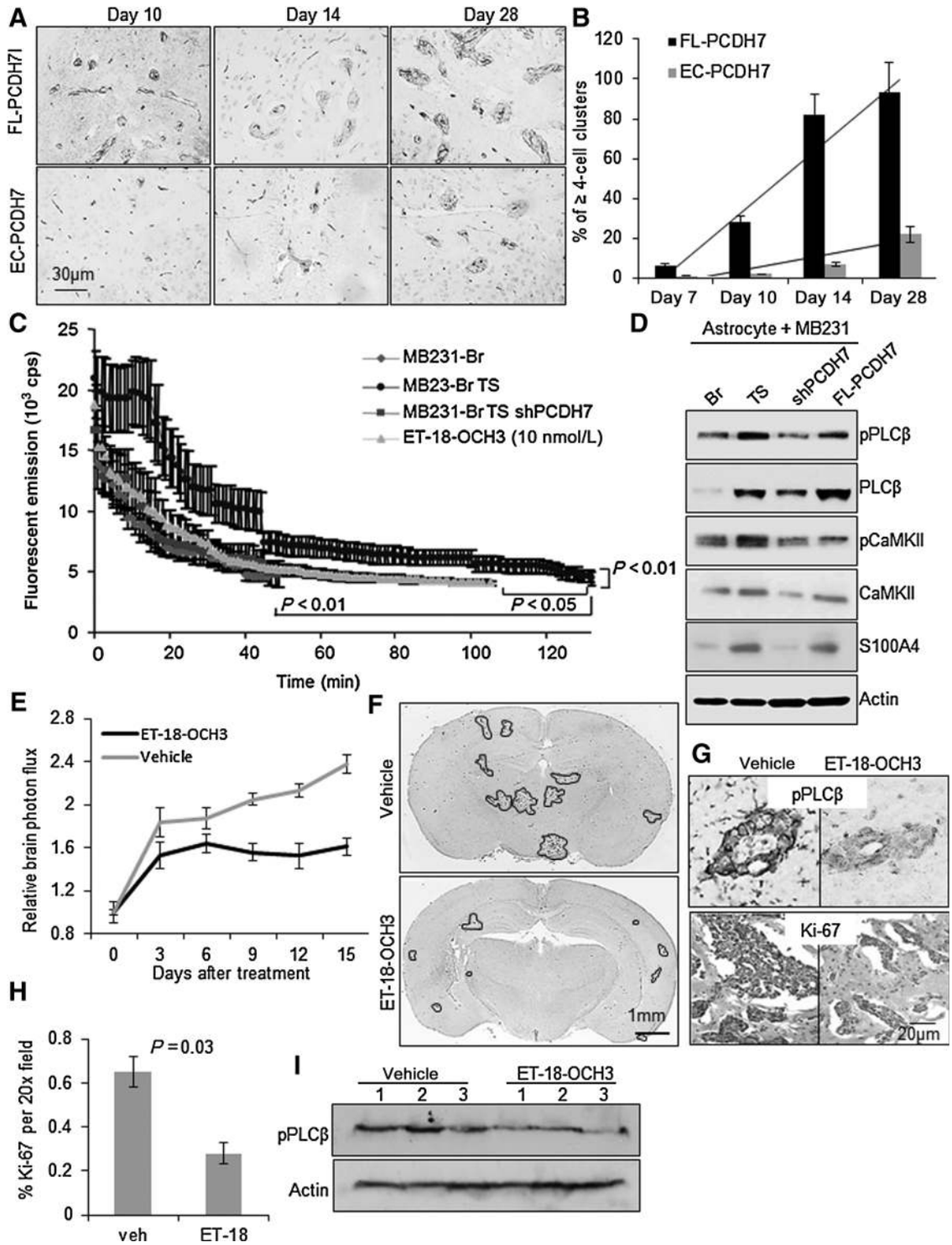

Figure 5.

Tumor–astrocyte interaction activates PCDH7-PLCβ-Ca^{2+} signaling to promote colonization. **A,** Representative IHC images of metastatic colonies in mouse brain sections with intracardiac injection of indicated cells. Tumor cells were visualized with anti-human CD44 antibody and blood vessels were visualized with anti-mouse CD34 antibody. **B,** Percent of ≥4-cell clusters located outside vessels at indicated days after tumor cell injection ($n = 3$ mice/time point/cell line). **C,** Baseline level of cytoplasmic Ca^{2+} in the indicated tumor cells measured by ratiometric emission of calcium-saturated Asante of the tumor cells when coculturing with astrocytes. **D,** Signal activity of PLCβ, CaMKII, and S100A in the indicated MB231 cells when coculturing with normal human astrocytes. **E,** *In vivo* effects of PLC selective inhibitor ET-18-OCH3 (i.p., 30 mg/kg, once daily) on brain metastatic tumor growth. $n = 10$ per group. $P = 0.04$, determined by ANOVA *post hoc* test. **F,** Representative whole-brain sections showing macrometastatic lesions of ET-18-OCH3 or vehicle-treated mice at the end of the treatment. **G,** Representative immunostained images of pPLCβ1 and Ki-67 in brain sections. **H,** Quantification of the percentage of Ki-67–positive tumor cells in the brain sections. $P = 0.03$, determined by Student *t* test. **I,** Western blot analysis of pPLCβ1 expression in mouse brain lysates. $N = 3$ per group.

Our research identified four aspects of PCDH7-mediated tumor–astrocyte interactions in promoting TNBC brain metastases. First, direct contacts between CSCs and astrocytes initiate the activation of PCDH7-PLCβ-Ca^{2+} signaling to promote tumor colonization. The cytoplasmic domain of PCDHs is structurally diverse, in contrast to the homology between classical cadherins (41), suggesting novel intracellular interactions and functions for each PCDH, but these are less studied. Our data indicate that the noncanonical Wnt/PLCβ-Ca^{2+} is a PCDH7 intracellular signaling event that is functionally critical to TNBC brain metastasis. Second, high-expression of PCDH7 in CSCs and astrocytes may mediate homophilic or heterophilic interactions of PCDH7 with other cadherin superfamily molecules in the same cells, neighboring cells, or both. For example, N-cadherin is highly expressed in neural tissue (41) and shares 35% sequence similarity with PCDH7 at EC1-2 domains, which could form a strand exchange trans-dimer with PCDH7 (Supplementary Table S3). In brain metastases from lung cancer patients, Grinberg–Rashi and colleagues reported that N-cadherin was significantly increased (42). We postulate that PCDH7-N-cadherin interactions can propagate N-cadherin signal transduction, such as EGFR-dependent migration signaling. Our previous work confirmed that genetic or pharmacologic inhibition of EGFR had profound anti-brain metastatic effects via suppressing PLC activity (43). Third, PCDH7 expression in breast and lung cancer cells has been shown to mediate the assembly of carcinoma–astrocyte gap junctions (10) in enabling the intercellular transmission of survival and apoptotic signals by which the activated astrocytes could protect tumor cells from chemotherapy (25). Coculturing with astrocytes induced upregulation of many prosurvival genes (*CCND1*, *BCL2L2*, and *CCNA1*) and downregulation of proapoptosis genes (*CASP8*, *LATS2*, *FAF1*, and *PDCD2*) in breast cancer cells (MDA-MB-231) even without chemotherapeutic treatment (Supplementary Fig. S3A; GSE26291), suggesting a proactive role of astrocytes in stimulating brain tumor growth. Finally, PCDHs are proteolitically processed by γ-secretase complex, releasing soluble intracellular fragments into cytoplasm, which might have a broad range of functions locally in the cytoplasm and/or even regulate gene expression similarly to other cell-surface proteins such as Notch and N-cadherin (44, 45).

Treatment for brain metastasis is an unmet medical need. Current treatment options, including radiotherapy, neurosurgery, and limited chemotherapy, frequently lead to treatment failure. Accumulated evidence has shown that elimination of CSCs is crucial in eradicating metastases (46, 47). In addition, elimination of stromal support by inhibiting feedback stimulation of cancer growth has shown antimetastatic efficacy and is the focus of many emerging therapies (48). As such, in our tumorsphere CSC animal studies, edelfosine almost completely eradicated the macrometastases in the mouse brain through inhibition of cell proliferation and breaching the astrocyte–tumor interplay. Edelfosine is a synthetic alkyl-lysophospholipid and a selective PLC inhibitor. It has been trialed in a phase II study for the treatment of brain cancer and showed encouraging results in stopping the tumor growth and a considerable improvement in the quality of life of the patients (US Patent 6514519). The drug incorporates into the cell membrane and does not target the DNA, thus it causes selective apoptosis in tumor cells, sparing healthy cells (49). While the existing treatment strategies for brain metastases are toxic to healthy tissues and significantly affect the patients' quality of life, our results indicate that further study of edelfosine as a potential treatment option for TNBC brain metastasis is warranted.

Disclosure of Potential Conflicts of Interest

No potential conflicts of interest were disclosed.

Authors' Contributions

Conception and design: D. Ren, X. Zhu, R. Kong, H. Zhao, S.T.C. Wong
Development of methodology: D. Ren, X. Zhu, R. Kong, Z. Zhao, K. Cui, H. Zhao, S.T.C. Wong
Acquisition of data (provided animals, acquired and managed patients, provided facilities, etc.): D. Ren, X. Zhu, Z. Zhao, X. Xu, K. Cui, H. Zhao
Analysis and interpretation of data (e.g., statistical analysis, biostatistics, computational analysis): D. Ren, R. Kong, Z. Zhao, X. Xu, J. Liu, X.H.-F. Zhang, H. Zhao, S.T.C. Wong
Writing, review, and/or revision of the manuscript: D. Ren, R. Kong, J. Wang, X. Xu, X.H.-F. Zhang, H. Zhao, S.T.C. Wong
Administrative, technical, or material support (i.e., reporting or organizing data, constructing databases): D. Ren, X. Xu, J. Liu, H. Zhao, S.T.C. Wong
Study supervision: H. Zhao, S.T.C. Wong

Acknowledgments

We thank all members of the Wong laboratory at Houston Methodist for discussions and assistance with data analysis; Drs. Neal Copeland and Jeffrey Rosen provided helpful comments for the manuscript; Drs. Rebecca Danforth and James Mancuso for their proofreading skills; and Drs. Patricia Steeg and Joan Massague generously provided MDA-MB-231-Br and CN34-Br cell lines. All microscopic imaging experiments were performed at Houston Methodist Research Institute's Advanced Cellular and Tissue Microscope Core Facility. We acknowledge the computational time funding support from the Texas Advanced Computing Center (TACC; Project ID: TG-MCB110130) at the University of Texas in Austin and BlueBioU (IBM POWER 7 Bioscience Computing Core at Rice University) to access super-computing resources. This research was funded by NIHU54 CA149196, NIHR01 CA121225, and John S. Dunn Research Foundation grants (to S.T. Wong), and R01-CA183878 (to X.H.-F. Zhang).

The costs of publication of this article were defrayed in part by the payment of page charges. This article must therefore be hereby marked *advertisement* in accordance with 18 U.S.C. Section 1734 solely to indicate this fact.

Received September 28, 2017; revised November 29, 2017; accepted February 15, 2018; published first March 22, 2018.

References

1. Qiu J, Xue X, Hu C, Xu H, Kou D, Li R, et al. Comparison of clinicopathological features and prognosis in triple-negative and non-triple negative breast cancer. J Cancer 2016;7:167–73.
2. Owonikoko TK, Arbiser J, Zelnak A, Shu HK, Shim H, Robin AM, et al. Current approaches to the treatment of metastatic brain tumours. Nat Rev Clin Oncol 2014;11:203–22.
3. Leone JP, Leone BA. Breast cancer brain metastases: the last frontier. Exp Hematol Oncol 2015;4:33.
4. Niikura N, Hayashi N, Masuda N, Takashima S, Nakamura R, Watanabe K, et al. Treatment outcomes and prognostic factors for patients with brain metastases from breast cancer of each subtype: a multicenter retrospective analysis. Breast Cancer Res Treat 2014;147:103–12.
5. Oskarsson T, Batlle E, Massague J. Metastatic stem cells: sources, niches, and vital pathways. Cell Stem Cell 2014;14:306–21.
6. Luzzi KJ, MacDonald IC, Schmidt EE, Kerkvliet N, Morris VL, Chambers AF, et al. Multistep nature of metastatic inefficiency: dormancy of solitary cells

after successful extravasation and limited survival of early micrometastases. Am J Pathol 1998;153:865–73.
7. Kienast Y, von Baumgarten L, Fuhrmann M, Klinkert WE, Goldbrunner R, Herms J, et al. Real-time imaging reveals the single steps of brain metastasis formation. Nat Med 2010;16:116–22.
8. Ye X, Tam WL, Shibue T, Kaygusuz Y, Reinhardt F, Ng Eaton E, et al. Distinct EMT programs control normal mammary stem cells and tumour-initiating cells. Nature 2015;525:256–60.
9. Lawson DA, Bhakta NR, Kessenbrock K, Prummel KD, Yu Y, Takai K, et al. Single-cell analysis reveals a stem-cell program in human metastatic breast cancer cells. Nature 2015;526:131–5.
10. Chen Q, Boire A, Jin X, Valiente M, Er EE, Lopez-Soto A, et al. Carcinoma-astrocyte gap junctions promote brain metastasis by cGAMP transfer. Nature 2016;533:493–8.
11. Tropepe V, Sibilia M, Ciruna BG, Rossant J, Wagner EF, van der Kooy D. Distinct neural stem cells proliferate in response to EGF and FGF in the developing mouse telencephalon. Dev Biol 1999;208:166–88.
12. Zhao H, Cui K, Nie F, Wang L, Brandl MB, Jin G, et al. The effect of mTOR inhibition alone or combined with MEK inhibitors on brain metastasis: an in vivo analysis in triple-negative breast cancer models. Breast Cancer Res Treat 2012;131:425–36.
13. Rota LM, Lazzarino DA, Ziegler AN, LeRoith D, Wood TL. Determining mammosphere-forming potential: application of the limiting dilution analysis. J Mammary Gland Biol Neoplasia 2012;17:119–23.
14. Bos PD, Zhang XH, Nadal C, Shu W, Gomis RR, Nguyen DX, et al. Genes that mediate breast cancer metastasis to the brain. Nature 2009; 459:1005–9.
15. Wu W, He Q, Li X, Zhang X, Lu A, Ge R, et al. Long-term cultured human neural stem cells undergo spontaneous transformation to tumor-initiating cells. Int J Biol Sci 2011;7:892–901.
16. Sihto H, Lundin J, Lundin M, Lehtimaki T, Ristimaki A, Holli K, et al. Breast cancer biological subtypes and protein expression predict for the preferential distant metastasis sites: a nationwide cohort study. Breast Cancer Res 2011;13:R87.
17. Jhanwar-Uniyal M, Labagnara M, Friedman M, Kwasnicki A, Murali R. Glioblastoma: molecular pathways, stem cells and therapeutic targets. Cancers 2015;7:538–55.
18. Guo L, Fan D, Zhang F, Price JE, Lee JS, Marchetti D, et al. Selection of brain metastasis-initiating breast cancer cells determined by growth on hard agar. Am J Pathol 2011;178:2357–66.
19. Clarke MF, Dick JE, Dirks PB, Eaves CJ, Jamieson CH, Jones DL, et al. Cancer stem cells–perspectives on current status and future directions: AACR Workshop on cancer stem cells. Cancer Res 2006;66:9339–44.
20. Wilhelm I, Molnar J, Fazakas C, Hasko J, Krizbai IA. Role of the blood-brain barrier in the formation of brain metastases. Int J Mol Sci 2013;14: 1383–411.
21. Cabrera MC, Hollingsworth RE, Hurt EM. Cancer stem cell plasticity and tumor hierarchy. World J Stem Cells 2015;7:27–36.
22. Sato N, Sanjuan IM, Heke M, Uchida M, Naef F, Brivanlou AH. Molecular signature of human embryonic stem cells and its comparison with the mouse. Dev Biol 2003;260:404–13.
23. Suzuki ST. Recent progress in protocadherin research. Exp Cell Res 2000;261:13–8.
24. Termini J, Neman J, Jandial R. Role of the neural niche in brain metastatic cancer. Cancer Res 2014;74:4011–5.
25. Lin Q, Balasubramanian K, Fan D, Kim SJ, Guo L, Wang H, et al. Reactive astrocytes protect melanoma cells from chemotherapy by sequestering intracellular calcium through gap junction communication channels. Neoplasia 2010;12:748–54.
26. Frank M, Kemler R. Protocadherins. Curr Opin Cell Biol 2002;14:557–62.
27. Jaffe LF. A calcium-based theory of carcinogenesis. Adv Cancer Res 2005;94:231–63.
28. Tonelli FM, Santos AK, Gomes DA, da Silva SL, Gomes KN, Ladeira LO, et al. Stem cells and calcium signaling. Adv Exp Med Biol 2012;740: 891–916.
29. Croker AK, Goodale D, Chu J, Postenka C, Hedley BD, Hess DA, et al. High aldehyde dehydrogenase and expression of cancer stem cell markers selects for breast cancer cells with enhanced malignant and metastatic ability. J Cell Mol Med 2009;13:2236–52.
30. Liu H, Patel MR, Prescher JA, Patsialou A, Qian D, Lin J, et al. Cancer stem cells from human breast tumors are involved in spontaneous metastases in orthotopic mouse models. Proc Natl Acad Sci U S A 2010;107:18115–20.
31. Fang X, Cai Y, Liu J, Wang Z, Wu Q, Zhang Z, et al. Twist2 contributes to breast cancer progression by promoting an epithelial-mesenchymal transition and cancer stem-like cell self-renewal. Oncogene 2011;30:4707–20.
32. Mani SA, Guo W, Liao MJ, Eaton EN, Ayyanan A, Zhou AY, et al. The epithelial-mesenchymal transition generates cells with properties of stem cells. Cell 2008;133:704–15.
33. Csermely P, Hodsagi J, Korcsmaros T, Modos D, Perez-Lopez AR, Szalay K, et al. Cancer stem cells display extremely large evolvability: alternating plastic and rigid networks as a potential Mechanism: network models, novel therapeutic target strategies, and the contributions of hypoxia, inflammation and cellular senescence. Semin Cancer Biol 2015;30:42–51.
34. Tirino V, Desiderio V, Paino F, De Rosa A, Papaccio F, La Noce M, et al. Cancer stem cells in solid tumors: an overview and new approaches for their isolation and characterization. FASEB J 2013;27:13–24.
35. Joyce JA, Pollard JW. Microenvironmental regulation of metastasis. Nat Rev Cancer 2009;9:239–52.
36. Zhang L, Zhang S, Yao J, Lowery FJ, Zhang Q, Huang WC, et al. Microenvironment-induced PTEN loss by exosomal microRNA primes brain metastasis outgrowth. Nature 2015;527:100–04.
37. Menachem A, Makovski V, Bodner O, Pasmanik-Chor M, Stein R, Shomron N, et al. Intercellular transfer of small RNAs from astrocytes to lung tumor cells induces resistance to chemotherapy. Oncotarget 2016;7:12489–504.
38. Aakula A, Kohonen P, Leivonen SK, Makela R, Hintsanen P, Mpindi JP, et al. Systematic identification of MicroRNAs that impact on proliferation of prostate cancer cells and display changed expression in tumor tissue. Eur Urol 2016;69:1120–8.
39. Jovicic A, Roshan R, Moisoi N, Pradervand S, Moser R, Pillai B, et al. Comprehensive expression analyses of neural cell-type-specific miRNAs identify new determinants of the specification and maintenance of neuronal phenotypes. J Neurosci 2013;33:5127–37.
40. Dolmetsch RE, Xu K, Lewis RS. Calcium oscillations increase the efficiency and specificity of gene expression. Nature 1998;392:933–6.
41. Halbleib JM, Nelson WJ. Cadherins in development: cell adhesion, sorting, and tissue morphogenesis. Genes Dev 2006;20:3199–214.
42. Grinberg-Rashi H, Ofek E, Perelman M, Skarda J, Yaron P, Hajduch M, et al. The expression of three genes in primary non-small cell lung cancer is associated with metastatic spread to the brain. Clin Cancer Res 2009;15: 1755–61.
43. Nie F, Yang J, Wen S, An YL, Ding J, Ju SH, et al. Involvement of epidermal growth factor receptor overexpression in the promotion of breast cancer brain metastasis. Cancer 2012;118:5198–209.
44. Bonn S, Seeburg PH, Schwarz MK. Combinatorial expression of alpha- and gamma-protocadherins alters their presenilin-dependent processing. Mol Cell Biol 2007;27:4121–32.
45. Buchanan SM, Schalm SS, Maniatis T. Proteolytic processing of protocadherin proteins requires endocytosis. Proc Natl Acad Sci U S A 2010;107: 17774–9.
46. Chen K, Huang YH, Chen JL. Understanding and targeting cancer stem cells: therapeutic implications and challenges. Acta Pharmacol Sin 2013; 34:732–40.
47. Dragu DL, Necula LG, Bleotu C, Diaconu CC, Chivu-Economescu M. Therapies targeting cancer stem cells: current trends and future challenges. World J Stem Cells 2015;7:1185–201.
48. Engels B, Rowley DA, Schreiber H. Targeting stroma to treat cancers. Semin Cancer Biol 2012;22:41–9.
49. Mollinedo F, Gajate C, Martin-Santamaria S, Gago F. ET-18-OCH3 (edelfosine): a selective antitumour lipid targeting apoptosis through intracellular activation of Fas/CD95 death receptor. Curr Med Chem 2004;11: 3163–84.
50. Roth RB, Hevezi P, Lee J, Willhite D, Lechner SM, Foster AC, et al. Gene expression analyses reveal molecular relationships among 20 regions of the human CNS. Neurogenetics 2006;7:67–80.